PROCEEDINGS OF THE ROYAL SOCIETY A MATHEMATICAL, PHYSICAL & ENGINEERING SCIENCES

Single- and double-spiral-vortex models for a supercavitating non-symmetric wedge in a jet

Y. A. Antipov and A. Y. Zemlyanova

Proc. R. Soc. A 2009 **465**, 3817-3837 first published online 25 September 2009
doi: 10.1098/rspa.2009.0251

PROCEEDINGS OF THE ROYAL SOCIETY A

Proc. R. Soc. A (2009) **465**, 3817–3837
doi:10.1098/rspa.2009.0251
Published online 25 September 2009

Single- and double-spiral-vortex models for a supercavitating non-symmetric wedge in a jet

By Y. A. Antipov* and A. Y. Zemlyanova

Department of Mathematics, Louisiana State University, Baton Rouge, LA 70803, USA

The problem of determining the free surface of a jet incident on a rigid wedge and the boundary of a cavity behind the wedge is considered. The single- and double-spiral-vortex models by Tulin are used to describe the flow at the rear part of the cavity. The location of the wedge in the jet and the sides lengths are arbitrary. This circumstance makes the flow domain doubly connected for the single-vortex model while it is simply connected for the double-vortex model. Both models are solved in closed form by the method of conformal mappings. The maps are expressed through the solutions to certain Riemann–Hilbert problems. For the former model, this problem is formulated on a genus-1 Riemann surface. The double-vortex model requires the solution to a standard Riemann–Hilbert problem on a plane. By comparative analysis of the numerical results for the two models, it is found that the drag and lift are practically the same while the jet surface, the cavity boundary at the rear part and the deflection angle of the jet at infinity are different. Also, the problem of determining the parameters for the conformal mapping in the single-vortex model has two solutions. It is shown that one of the solutions leads to a non-physical shape of the cavity and needs to be disregarded.

Keywords: conformal mapping; Riemann–Hilbert problem; free boundary

1. Introduction

It is a relatively easy matter to solve a problem of two-dimensional, irrotational, incompressible, steady flow past a polygonal obstacle with rigid walls when the flow domain is simply connected and its boundary is prescribed. It is more difficult to deal with non-symmetric flow when the boundary of the flow domain is free and the model assumes the existence of a cavity behind the body. Because flow is unsteady at the rear part of the cavity, any steady-state model of supercavitating flow is approximate. The most successful steady-state cavity closure models achieve a reasonable balance between the mathematical rigorousness and experimental observations and allow to apply the theory of functions of a complex variable and derive an analytical solution.

The models of supercavitating flow used in the literature are described by Gilbarg (1960), Wu (1972), Gurevich (1979) and Brennen (1985). These models include the Joukowsky open-wake model, the Riabouchinsky image model,

*Author for correspondence (antipov@math.lsu.edu).

Received 8 May 2009
Accepted 24 August 2009

the Efros–Gilbarg–Rock–Kreisel re-entrant jet model and the two spiral-vortex models by Tulin (1964). The open wake model assumes the existence of a semi-infinite wake behind the obstacle. Riaboushinsky proposed to place an image obstacle downstream of the real body. In the re-entrant jet model, the flow domain is a two-sheeted Riemann surface formed by gluing two replicas of the physical plane along the hydrofoil. It is assumed that a part of the main stream reverses the direction and proceeds to the second sheet through the junction line of the Riemann surface.

In the Tulin spiral-vortex models, there are two vortices in the rear part of the cavity. The single-spiral-vortex model assumes that the velocity is continuous at the centres of the vortices but the two branches which form the cavity boundary are discontinuous in the physical plane (according to the Terent'ev's (1981) interpretation the flow can be considered on a half of the infinitely sheeted Riemann surface of a logarithmic function whose branch points are the centres of the vortices). In the double-spiral-vortex model, the speed is discontinuous at the vortices and there is a semi-infinite wake behind the cavity. The speed on the wake boundary is constant and is the same as at infinity. From the mathematical point of view, there are two features that distinguish these two models. First, the complex velocity potential, w, has different asymptotics at the centres, C_j, of the vortices. For the single-spiral-vortex model, $\ln \mathrm{d}w/\mathrm{d}z = \mathrm{O}\{[w - w(C_j)]^{-1/2}\}$, and for the double-spiral-vortex model, $\ln \mathrm{d}w/\mathrm{d}z = \mathrm{O}\{\ln[w - w(C_j)]\}$, $z \to C_j$. Another difference is that for the former model, apart from some particular cases, the flow domain is multiply connected. In the second model, the flow domain is always simply connected. The double-spiral-vortex model was used by Larock & Street (1967) for the analysis of a cavitating foil beneath a free surface, by Bassanini & Elcrat (1988) in the case of a cavitating polygonal plate in a plane and Furuya (1975) in a numerical scheme for the a cavitating foil of an arbitrary shape. For simply connected flow domains, the nonlinear single-spiral-vortex model was employed by Larock & Street (1975), Terent'ev (1976) and Gurevich (1979). By using the same model and the method of Riemann surfaces, Antipov & Silvestrov (2007, 2008) analysed the case of two foils in a channel, and a wedge with a trailing and a partial cavity in a plane. A method of the Riemann–Hilbert problem for piece-wise automorphic functions for supercavitating flow in an $n+1$-connected flow domain was proposed by Antipov & Silvestrov (2009). We emphasize that in these papers, the numerical computations were implemented for the simply connected case only. The single-spiral-vortex model was employed by Terent'ev (1981) to find an asymptotic solution for small angles of attack for a supercavitating hydrofoil beneath a free surface. Antipov & Zemlyanova (2009) solved analytically the problem of supercavitating flow of a wedge beneath a free surface.

To the knowledge of the authors, neither Tulin's model has been applied to the study of a jet past a supercavitating non-symmetric wedge. The work presented herein is intended as a comparative study of the single- and double-spiral-vortex models applied to supercavitating jet flow past a wedge when the location and the side lengths of the wedge are arbitrary. Recently, Kawakami *et al.* (2009) carried out some experiments in the high-speed water tunnel at St Anthony Falls Laboratory to study the ventilated supercavity formed behind a sharp-edged disk. They found that the dominant mode of the cavity-closure mechanism is the twin vortex mode while the re-entrant jet mode has been found to be unstable. This provides additional impetus to study the Tulin twin vortices models.

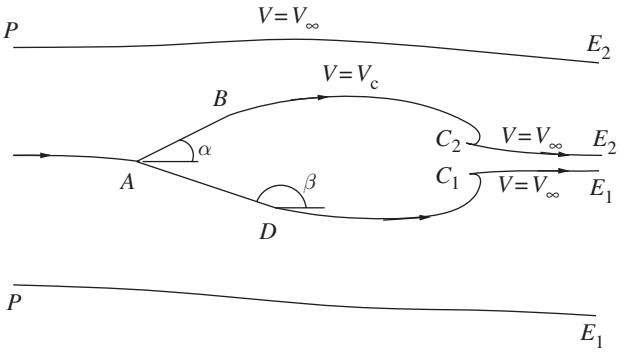

Figure 1. The double-spiral-vortex model domain.

2. Double-spiral-vortex model

(*a*) *Formulation*

The flow is two-dimensional, incompressible and irrotational, and the gravity is neglected. The vertex, A, of the wedge, DAB, is fixed and is chosen to be the origin of the plane $z = x_1 + ix_2$ (figure 1). Far away from the wedge, as $x_1 \to -\infty$, the upper and the lower free surfaces of the jet are described by the equations $x_2 = h_1$ and $x_2 = -h + h_1$, respectively. As $x_1 \to -\infty$, the velocity of the flow is also prescribed, $\mathbf{v} = (V_\infty, 0)$. The upper and the lower sides of the wedge have lengths λ_1 and λ_2, and the angles they form with the x_1-axis are α_0 and β_0, respectively. A motion with the following features is to be considered.

(i) The wedge may move about the x_3-axis orthogonal to the flow plane. The angle of yaw, δ, is to be determined from the condition that the vertex A is the only stagnation point of the flow.

(ii) The sides of the wedge are straight and rigid. The flow branches at the point A, and the velocity vector is tangent to the faces of the wedge,

$$\arg \frac{\mathrm{d}w}{\mathrm{d}z} = \begin{cases} -\alpha, & z \in AB, \\ \pi - \beta, & z \in AD, \end{cases} \tag{2.1}$$

where $\alpha = \alpha_0 + \delta$ and $\beta = \beta_0 + \delta$. These two angles define the actual position of the wedge when the flow is in a steady state. The derivative $\overline{\mathrm{d}w/\mathrm{d}z} = v_1 + iv_2$ is the complex velocity, v_1 and v_2 are the components of the velocity vector $\mathbf{v}$ and $w(z) = \phi(z) + i\psi(z)$ is a complex potential of the flow.

(iii) Behind the wedge, there is a cavity formed by two branches, ABC_2 and ADC_1, of the same streamline. The cavity pressure, p_c, is constant and prescribed. The flow separates smoothly from the points B and D. The free streamlines ABC_2 and ADC_1 form two spirals at the ending points C_2 and C_1. The speed on the boundary of the cavity is constant, $V = V_c$, where $V_c = \sqrt{\sigma + 1}\, V_\infty$, σ is the cavitation number, $\sigma = 2(p_\infty - p_c)(\rho V_\infty^2)^{-1}$, ρ is the density of the liquid and p_∞ is the pressure as $x_1 \to -\infty$. At the centres of the spiral vortices, C_1 and C_2, the logarithm of the complex

velocity has the following singularity (Tulin 1964):

$$\ln\frac{\mathrm{d}w}{\mathrm{d}z}=\mathrm{O}\left\{\ln[w-w(C_j)]\right\},\quad z\to C_j,\ \ j=1,2. \tag{2.2}$$

At the points C_j, the speed is discontinuous. First, the streamlines spiral at speed V_c, then the speed jumps to $V=V_\infty$, and the streamlines spiral backwards and continue in the direction of the infinite point $+\infty+ix_2$ (x_2 is finite) forming a wake. Thus, we have

$$\left.\begin{aligned}&\left|\frac{\mathrm{d}w}{\mathrm{d}z}\right|=\begin{cases}V_c, & z\in BC_2\cup DC_1,\\ V_\infty, & z\in C_2E_2\cup C_1E_1,\end{cases}\\ \text{and}\qquad &\operatorname{Im}w(z)=\psi_0,\quad z\in ABC_2E_2\cup ADC_1E_1,\ \ \psi_0=\text{const.}\end{aligned}\right\} \tag{2.3}$$

(iv) The boundary of the free surfaces of the jet is formed by two streamlines, PE_2 and PE_1, and the speed on the free surfaces is assumed to be constant $V=V_\infty$. Thus,

$$\left.\begin{aligned}&\left|\frac{\mathrm{d}w}{\mathrm{d}z}\right|=V_\infty,\quad z\in PE_1\cup PE_2,\\ \text{and}\qquad &\operatorname{Im}w(z)=\begin{cases}-\psi_1, & z\in PE_1,\\ \psi_2, & z\in PE_2,\end{cases}\quad \psi_j=\text{const.}\ \ j=1,2.\end{aligned}\right\} \tag{2.4}$$

(v) The complex potential $w(z)$ has the same values at the centres of the double spirals, the points C_1 and C_2 (Larock & Street 1967) or, equivalently,

$$\operatorname{Re}w(C_1)=\operatorname{Re}w(C_2). \tag{2.5}$$

(vi) The width of the jet is finite as $x_1\to+\infty$. This condition means that

$$\arg\frac{\mathrm{d}w}{\mathrm{d}z}\bigg|_{z=E_1}=\arg\frac{\mathrm{d}w}{\mathrm{d}z}\bigg|_{z=E_2}. \tag{2.6}$$

(*b*) *Conformal mapping*

The double-spiral-vortex model of supercavitating flow of a jet past n finite obstacles is flow in a simply connected domain regardless of the number n. Therefore, there exists a function $z=f(\zeta)$ that maps conformally a half-plane into the flow domain. We denote the pre-images of the points A, B, C_j, D, E_j and P by a, b, c_j, d, e_j and p, respectively (figure 2*a*). Three real parameters can be fixed arbitrarily, and we choose $a=0$, $d=-1$ and $p=\infty$.

To derive the expression of the mapping function $f(\zeta)$, we represent its derivative in the form

$$\frac{\mathrm{d}f}{\mathrm{d}\zeta}=\frac{\omega_0(\zeta)}{V_\infty}\mathrm{e}^{-\omega_1(\zeta)}, \tag{2.7}$$

where

$$\omega_0(\zeta)=\frac{\mathrm{d}w}{\mathrm{d}\zeta},\quad \omega_1(\zeta)=\ln\frac{\mathrm{d}w}{V_\infty\mathrm{d}z}. \tag{2.8}$$

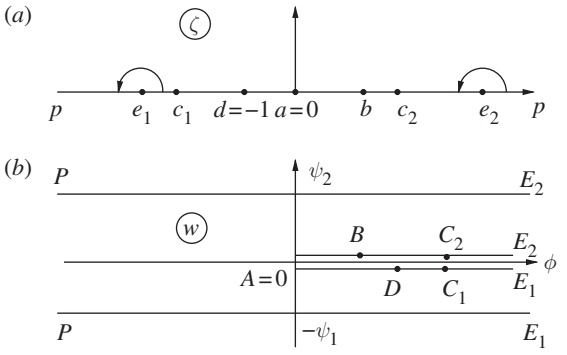

Figure 2. The parametric (*a*) and hodograph (*b*) planes.

The standard Schwarz–Christoffel formula is employed to recover the function $\omega_0(\zeta)$,

$$\omega_0(\zeta) = \frac{q_1\zeta}{(\zeta - e_1)(\zeta - e_2)}. \tag{2.9}$$

By integrating this expression, we find the complex potential $w(z(\zeta))$

$$w = \frac{q_1}{e_1 - e_2}\left[e_1 \ln(\zeta - e_1) - e_2 \ln(\zeta - e_2)\right] + q_2. \tag{2.10}$$

Here, $\ln(\zeta - e_j)$ are the branches fixed by the condition $0 \leq \arg(\zeta - e_j) < \pi$, and q_1 and q_2 are some constants. To fix these constants, in addition to the parametric ζ-plane, consider the w-plane (figure 2*b*). As $w(0) = 0$, we may find that

$$q_2 = -\frac{q_1}{e_1 - e_2}\left[e_1 \ln(-e_1) - e_2(\ln e_2 + i\pi)\right]. \tag{2.11}$$

Determine now the constant q_1. Notice that as a point ζ traverses around the point $\zeta = e_j$ $(j = 1, 2)$ along a path in the upper half-plane (figure 2*a*), the variation of the function $\ln(\zeta - e_j)$ is $i\pi$ while the corresponding variation of w is $-i\psi_j$ (figure 2*b*). Consequently, $q_1 = -(\psi_1 + \psi_2)/\pi$, $e_1 = -\psi_1 e_2/\psi_2$. The use of the conservation of mass law defines the constants ψ_1 and ψ_2: $\psi_1 = V_\infty(h - h_1)$, $\psi_2 = V_\infty h_1$. Thus, the function $\omega_0(\zeta)$ is defined by the expression

$$\omega_0(\zeta) = -\frac{V_\infty h\zeta}{\pi[\zeta - (1 - h/h_1)e_2](\zeta - e_2)} \tag{2.12}$$

which possesses one unknown real parameter e_2.

We turn now to the determination of the function $\omega_1(\zeta)$. On referring to the boundary conditions (2.1), (2.3) and (2.4), we see from equation (2.8) that

$$\left.\begin{aligned} &\operatorname{Re}\omega_1(\xi) = 0, \quad \xi \in pe_1 \cup e_1c_1 \cup c_2e_2 \cup e_2p, \\ &\operatorname{Re}\omega_1(\xi) = \frac{1}{2}\ln(1 + \sigma), \quad \xi \in c_1d \cup bc_2, \\ \text{and} \quad &\operatorname{Im}\omega_1(\xi) = -\alpha, \ \ \xi \in ab; \quad \operatorname{Im}\omega_1(\xi) = \pi - \beta, \ \ \xi \in da. \end{aligned}\right\} \tag{2.13}$$

It will be convenient to introduce an auxiliary function, $\Phi(\zeta)$, defined in the whole ζ-plane by

$$\Phi(\zeta)=\begin{cases}-i\omega_1(\zeta), & \operatorname{Im}\zeta>0,\\ i\,\overline{\omega_1(\bar{\zeta})}, & \operatorname{Im}\zeta<0.\end{cases} \tag{2.14}$$

From the boundary conditions (2.13), we see that the function $\Phi(\zeta)$ represents the solution to the following Riemann–Hilbert problem for symmetric functions.

Find all functions $\Phi(\zeta)$ analytic in the upper and lower half-planes, Hölder-continuous up to the real axis except for the points $a=0$, b, $d=-1$, c_1 and c_2 whose one-sided limits, $\Phi^+(\xi)$ and $\Phi^-(\xi)$, satisfy the following boundary condition:

$$\Phi^+(\xi)=G(\xi)\Phi^-(\xi)+g(\xi),\quad -\infty<\xi<+\infty, \tag{2.15}$$

where

$$G(\xi)=\begin{cases}1, & \xi\in pd\cup bp,\\ -1, & \xi\in db,\end{cases}\qquad g(\xi)=\begin{cases}0, & \xi\in pc_1\cup c_2p,\\ -i\ln(1+\sigma), & \xi\in c_1d\cup bc_2,\\ -2\alpha, & \xi\in ab,\\ 2(\pi-\beta), & \xi\in da.\end{cases} \tag{2.16}$$

The function $\Phi(\zeta)$ is symmetric, $\Phi(\zeta)=\overline{\Phi(\bar{\zeta})}$, bounded at the points b and $d=-1$ and may have logarithmic singularities at the points $a=0$, c_1 and c_2. At the point $p=\infty$, it vanishes.

To factorize the coefficient $G(\xi)$, we use the function $\chi(\zeta)=\sqrt{(\zeta-b)(\zeta+1)}$, single valued in the ζ-plane cut along the segment $[-1,b]$. The branch is fixed by the condition $\chi(\xi)>0$, $\xi>b$. In the class of functions bounded at the points b, $d=-1$, and $p=\infty$, the solution is unique and given by

$$\Phi(\zeta)=\frac{\chi(\zeta)}{2\pi i}\int_{c_1}^{c_2}\frac{g(\xi)\,\mathrm{d}\xi}{\chi^+(\xi)(\xi-\zeta)}. \tag{2.17}$$

It vanishes at the point p if and only if

$$\int_{c_1}^{c_2}\frac{g(\xi)\,\mathrm{d}\xi}{\chi^+(\xi)}=0. \tag{2.18}$$

By computing the integral in equation (2.18), we obtain the following real condition for the unknown parameters of the mapping

$$-\ln(1+\sigma)\ln\frac{2\chi^+(c_2)+2c_2-b+1}{-2\chi^+(c_1)-2c_1+b-1}+2\alpha\rho^--2(\pi-\beta)\rho^+=0, \tag{2.19}$$

where

$$\rho^\pm=\frac{\pi}{2}\pm\sin^{-1}\frac{1-b}{1+b}. \tag{2.20}$$

The singular integral (2.17) is evaluated in appendix A. The final formula for the function $\Phi(z)$ becomes

$$\Phi(\zeta)=\frac{\ln(1+\sigma)}{2\pi}\left(\ln\frac{\rho_1-\hat{\zeta}}{\rho_1+\hat{\zeta}}-\ln\frac{\rho_2-1/\hat{\zeta}}{\rho_2+1/\hat{\zeta}}\right)-\alpha-\frac{i(\pi+\alpha-\beta)}{\pi}\ln\frac{\sqrt{b}+i\hat{\zeta}}{\sqrt{b}-i\hat{\zeta}}, \tag{2.21}$$

where the functions $\hat{\zeta}$, ρ_1 and ρ_2 are defined in appendix A.

(*c*) *Definition of the parameters and numerical results*

The derivative of the conformal mapping equation (2.7) has been expressed through the functions $\omega_0(\zeta)$ and $\omega_1(\zeta) = i\Phi(\zeta)$, $\operatorname{Im}\zeta > 0$, given by equations (2.12) and (2.21). It will be convenient to rewrite its expression in the form

$$\frac{\mathrm{d}f}{\mathrm{d}\zeta} = hF(\zeta), \quad F(\zeta) = -\frac{\zeta\, e^{-\omega_1(\zeta)}}{\pi(\zeta - e_1)(\zeta - e_2)}. \tag{2.22}$$

The function $F(\zeta)$ has five unknown real parameters, e_2, c_1, c_2 and b, the pre-images of the points E_2, C_1, C_2 and B, as well as the yaw angle δ. The parameter e_1 is expressed through the unknown e_2 by

$$e_1 = \frac{l-1}{l}e_2, \quad l = h_1/h \in (0,1). \tag{2.23}$$

For the definition of these five parameters, we have the condition (2.19), the following two geometric conditions:

$$\operatorname{Im}\int_0^b F(\zeta)\,\mathrm{d}\zeta = \lambda_1^\circ \sin\alpha \quad \text{and} \quad \operatorname{Im}\int_{-1}^0 F(\zeta)\,\mathrm{d}\zeta = \lambda_2^\circ \sin\beta, \;\; \lambda_j^\circ = \frac{\lambda_j}{h}, \tag{2.24}$$

and the relations

$$\left.\begin{aligned} \ln\frac{c_1 - e_1}{c_2 - e_1} &= \frac{e_2}{e_1}\ln\frac{e_2 - c_1}{e_2 - c_2} \\ \text{and} \qquad \operatorname{Im}\omega_1(e_1) &= \operatorname{Im}\omega_1(e_2). \end{aligned}\right\} \tag{2.25}$$

The last two conditions follow from equations (2.5) and (2.6) of the model. Notice that equation (2.19) and the second equation in (2.25) are linear with respect to the parameter δ. This makes it possible to express this parameter from one of these two equations, say, equation (2.19), through the other four parameters, b, c_1, c_2 and e_2. For the solution of the system of the four nonlinear equations (2.24) and (2.25), we use a scheme based on the Newton iterative method (Antipov & Zemlyanova 2009).

Because the derivative of the conformal mapping has been found, it is possible to reconstruct the free boundary that consists of the jet surface, the cavity and the wake profile. By integrating the function $\mathrm{d}f/\mathrm{d}\zeta$, we obtain the lower and upper boundaries of the jet,

$$\left.\begin{aligned} z(\tau) &= D + \int_{d\tau}\frac{\mathrm{d}f}{\mathrm{d}\zeta}\mathrm{d}\zeta, \quad \tau \in pe_1 (z \in PE_1), \\ \text{and} \qquad z(\tau) &= B + \int_{b\tau}\frac{\mathrm{d}f}{\mathrm{d}\zeta}\mathrm{d}\zeta, \quad \tau \in pe_2 (z \in PE_2). \end{aligned}\right\} \tag{2.26}$$

For the cavity and wake boundaries, we have similar formulas. For the lower part of the cavity boundary, $\tau \in dc_1$ ($z \in DC_1$) and for the upper one, $\tau \in bc_2$ ($z \in BC_2$). Figure 3 shows the cavity shape and the profile of the wake and the jet when $\lambda_1^\circ = \lambda_2^\circ = 1/16$, $l = 5/8$ and $\alpha_0 = \pi - \beta_0 = \pi/3$ for the values 0.4, 0.5 and 1 of the

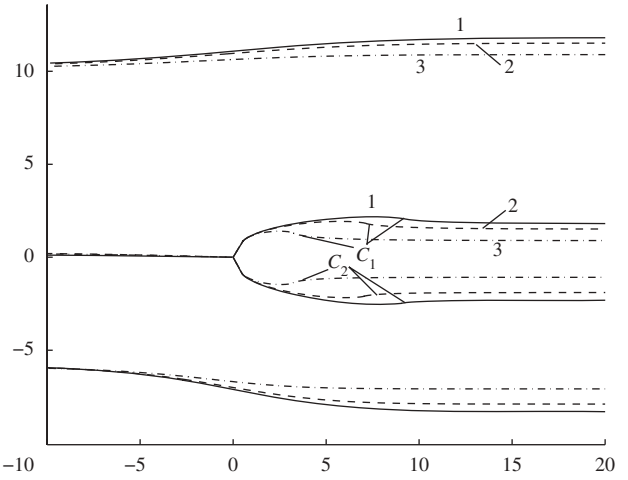

Figure 3. The cavity, wake and jet profiles when $\lambda_1 = \lambda_2 = 1$, $h = 16$, $h_1 = 10$, $\alpha_0 = \pi/3$ and $\beta_0 = 2\pi/3$ for some values of the cavitation parameter σ: $\sigma = 0.4$ (1), $\sigma = 0.5$ (2) and $\sigma = 1$ (3).

cavitation number σ. The parameters of the conformal mapping for $\sigma = 1$ have the following values: $e_1 = -1.82018$, $c_1 = -1.74692$, $b = 1.18188$, $c_2 = 2.62667$ and $e_2 = 3.03363$. It is seen that the cavity size and the width of the wake behind the cavity increase when the cavitation number decreases. When $\alpha_0 + \beta_0$ and the angle of attack are not small while the cavitation number is small, the model reminisces the Joukowsky open wake model. In this case it is worth replacing equation (2.5) (the zero circulation condition) by the condition $h_w = 0$, where h_w is the thickness of the wake at infinity. This guarantees the closure of the wake at infinity (Tulin 1964).

We proceed now to compute the drag and lift coefficients

$$C_X + iC_Y = \frac{2(X + iY)}{\rho V_\infty^2 \lambda^\circ h}, \tag{2.27}$$

where $\lambda^\circ = \lambda_1^\circ \sin\alpha + \lambda_2^\circ \sin\beta$, X and Y are drag and lift, respectively, which by Bernoulli's law can be represented in the form

$$X + iY = -\frac{i\rho}{2} \int_{DAB} (V_c^2 - V^2)\, \mathrm{d}z, \tag{2.28}$$

where $V = |\mathrm{d}w/\mathrm{d}z|$. We have finally

$$C_X + iC_Y = -\frac{i}{\lambda^\circ} \int_{dab} [\sigma + 1 - e^{2\,\mathrm{Re}\,\omega_1(\zeta)}] F(\zeta)\, \mathrm{d}\zeta. \tag{2.29}$$

For the parameters $\alpha_0 = \pi - \beta_0 = \pi/3$, $\lambda_1^\circ = 0.05$, $\lambda_2^\circ = 0.1$ and $l = 0.5$, the drag and lift coefficients increase when the cavitation number σ increases (figure 4).

Our scheme applied to a single hydrofoil for small $l = h_1/h$ is consistent with the results of Larock & Street (1967) for the coefficient $C_D + iC_L = \lambda^\circ(\lambda_1^\circ + \lambda_2^\circ)^{-1}(C_X + iC_Y)$ obtained for a foil beneath a free surface ($h_1 = 1$, $h = \infty$).

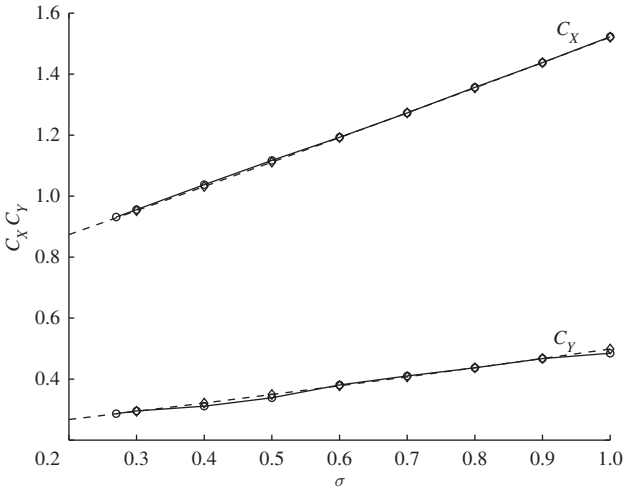

Figure 4. The drag and lift coefficients, C_X and C_Y, when $\lambda_1 = 1$, $\lambda_2 = 2$, $h = 20$, $h_1 = 10$ and $\alpha_0 = \pi - \beta_0 = \pi/3$ versus the parameter σ: the single-spiral-vortex model (solid line) and the double-spiral-vortex model (dashed line).

For $h = 1000$ and $h_1 = 1$, the angle of attack 5.66° and $\sigma = 0.096$, the coefficient $C_D + iC_L$ obtained from our jet solution is $0.0190037 + i0.191522$, and the one reported by Larock and Street is $0.019 + i0.191$.

3. Single-spiral-vortex model

(*a*) *Description of the model*

The first two assumptions, (i) and (ii), of the single-spiral-vortex model are the same as for the double-spiral-vortex model described in §2*a*. We write down the other assumptions of the model that distinguish this model from the double-spiral-vortex model.

(iii) The closure cavity mechanism for the single-spiral-vortex model is different from equation (2.2), and is described by Terent'ev (1976)

$$\log \frac{\mathrm{d}w}{\mathrm{d}z} \sim -K((w - w(C))^{-1/2}), \quad z \to C, \ -\pi \le \arg[w(z) - w(C)] \le \pi. \tag{3.1}$$

Here K is a positive constant, and the branch of the square root is chosen such that $[w(z) - w(C)]^{1/2} > 0$ when $\arg[w(z) - w(C)] = 0$. According to the Terent'ev (1981) interpretation of the Tulin single-spiral-vortex model, the two branches of the dividing streamline at the centres of the vortices behind the foil, C_1 and C_2, pass to a half of an infinitely sheeted Riemann surface of the logarithmic function with the branch points C_1 and C_2. After that, the same streamline emerges from the infinite sheet of the Riemann surface and returns to a point C of the first, physical, sheet. In contrast to the double-spiral-vortex model, the speed is continuous at the rear part of the cavity (figure 5).

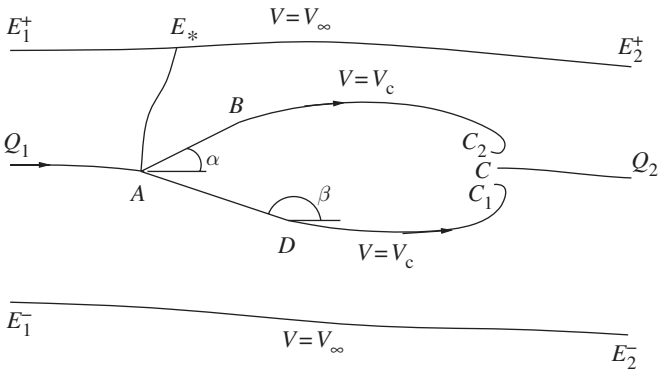

Figure 5. The single-spiral-vortex model domain $\tilde{\mathcal{D}}$.

On the boundary of the cavity, the complex potential $w(z)$ satisfies the following boundary conditions:

$$\left.\begin{aligned} &\operatorname{Im} w(z) = K_0, \quad z \in L_1, \\ \text{and} \quad &\left|\frac{\mathrm{d}w}{\mathrm{d}z}\right| = \begin{cases} V_\infty, & z \in L_0, \\ V_c, & z \in BC^+ \cup DC^-, \end{cases} \end{aligned}\right\} \tag{3.2}$$

where K_0 is a real constant, and the contour L_1 consists of the boundary of the cavity $BC_2 \cup DC_1$ and the faces of the wedge DAB.

(iv) On the jet surface $L_0 = E_1^- E_2^- \cup E_1^+ E_2^+$,

$$\operatorname{Im} w(z) = K_1^{\pm}, \quad z \in E_1^{\pm} E_2^{\pm}, \tag{3.3}$$

where K_1^+ and K_1^- are some real constants.

(v) By contrast with the double-spiral-vortex model, the flow domain, $\tilde{\mathcal{D}}$, is not simply connected but doubly connected. To assure that the flow is single valued, it is required that

$$\int_{L_*} \mathrm{d}z = 0. \tag{3.4}$$

Here L_* is a closed contour in the flow domain exterior to the contour L_1.

As for the double-spiral-vortex model, we use the conformal mapping technique. Let $z = f(\zeta)$ map the exterior of two cuts, $l_1 = [0, 1]$ and $l_0 = [m, \infty)$ onto the physical domain $\tilde{D}$ (figure 6). Here $m \in (1, +\infty)$ is a parameter to be fixed. Denote the pre-images of the points A, B, C, D, $E_1^{\pm}$ and $E_2^{\pm}$ by a, b, c, d, e_1 and e_2, respectively. Since such a map is defined up to one real parameter and since $e_1 \neq e_2$, we choose $e_1 = \bar{e}_2$. Clearly, two cases need to be considered, $e_1 = e_0 + i0$ and $e_1 = e_0 - i0$, where $e_0 = |e_1| = |e_2|$, $e_0 \in (m, +\infty)$.

As before, the derivative $\mathrm{d}f/\mathrm{d}\zeta$ is conveniently represented in terms of two functions, $\omega_0(\zeta)$ and $\omega_1(\zeta)$, by equation (2.7).

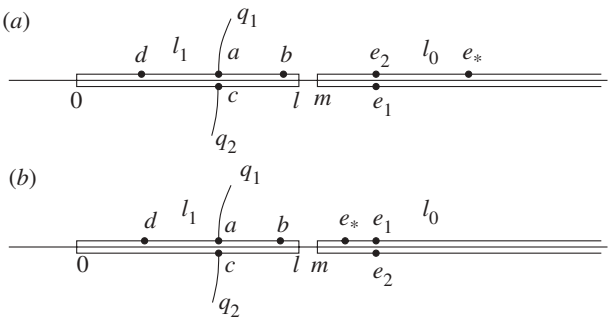

Figure 6. The parametric ζ-plane when $e_1 \in l_0^-$ (*a*) and $e_1 \in l_0^+$ (*b*).

(*b*) *Function* $\omega_0(\zeta)$

The function $\omega_0(\zeta)$ is analytic in the exterior of the cuts l_0 and l_1. At infinity, the function $f(\zeta)$ decays as $\tilde{K}\zeta^{-1/2}$, $\tilde{K} = \text{const}$. This implies $\omega_0(\zeta) = \mathrm{O}(\zeta^{-3/2})$, $\zeta \to \infty$. At the pre-images of the points $E_j^{\pm}$, it has a logarithmic singularity, $f(\zeta) \sim h\pi^{-1}(-1)^{j-1}\ln(\zeta - e_0)$, $j = 1, 2$. Since $\mathrm{d}w/\mathrm{d}z \sim V_\infty$, $\zeta \to e_1$, we obtain $\omega_0(\zeta) \sim hV_\infty[\pi(\zeta - e_0)]^{-1}$, $\zeta \to e_1$. It has been shown by Antipov & Silvestrov (2008) that the function $\mathrm{d}w/\mathrm{d}\zeta$ has to vanish at the stagnation point and the point where the branched streamline emerges from the Riemann surface of flow. In our case, this means that $\omega_0(\zeta)$ has simple zeros at the points a and c. Because of the first condition in equation (3.2) and (3.3), $\operatorname{Im}\omega_0(\zeta) = 0$ on l_0 and l_1. All these conditions can be written as a homogeneous Riemann–Hilbert problem. By solving it, we find that $a = \bar{c}$. Without loss of generality, we assume that $a \in l_1^+$ and then $c \in l_1^-$. The most general form of the function $\omega_0(\zeta)$ with such properties is

$$\omega_0(\zeta) = hV_\infty \omega_0^*(\zeta), \tag{3.5}$$

where

$$\omega_0^*(\zeta) = \frac{p^{1/2}(e_1)}{\pi p^{1/2}(\zeta)}\left(\frac{1}{\zeta - e_0} - \frac{1}{a - e_0}\right). \tag{3.6}$$

Here $p(\zeta) = \zeta(1-\zeta)(\zeta - m)$ and $p^{1/2}(\zeta)$ is the branch fixed by the condition $p^{1/2}(\xi) > 0$ if $\xi < 0$. At the banks of the cuts l_0 and l_1, $\zeta = \xi \pm i0$, it has the properties $p^{1/2}(\zeta) = \mp i|p^{1/2}(\xi)|$, $0 < \xi < 1$, and $p^{1/2}(\zeta) = \pm i|p^{1/2}(\xi)|$, $m < \xi < +\infty$. If $1 < \xi < m$, then the function $p^{1/2}(\xi)$ is negative.

The function $\omega_0(\zeta)$ has three real parameters, a, e_0 and m, to be determined. By conservation of mass, we can write down the first real condition for them

$$\operatorname{Im}\int_a^{e_*} \omega_0(\zeta)\,\mathrm{d}\zeta = h_1 V_\infty, \tag{3.7}$$

where e_* is the pre-image of a point E_* in the upper boundary of the jet. This condition can be transformed into the form

$$\operatorname{Im}\int_1^m \omega_0^*(\zeta)\,\mathrm{d}\zeta = \begin{cases} l-1, & e_1 \in l_0^-, \\ l, & e_1 \in l_0^+. \end{cases} \tag{3.8}$$

(c) Function $\omega_1(\zeta)$

From the conditions (2.1) and (3.1) to (3.3), we conclude that the function $\omega_1(\zeta)$ satisfies the boundary conditions

$$\left.\begin{aligned} \operatorname{Re}\omega_1(\zeta) &= \begin{cases} \log\sqrt{\sigma+1}, & \zeta\in bcd,\\ 0, & \zeta\in l_1, \end{cases}\\ \text{and}\qquad \operatorname{Im}\omega_1(\zeta) &= \begin{cases} -\alpha, & \zeta\in ab,\\ \pi-\beta, & \zeta\in da, \end{cases} \end{aligned}\right\} \tag{3.9}$$

and as $\zeta\to c$, $\omega_1(\zeta)=\mathrm{O}(1/(z-c))$. The function $\omega_1(\zeta)$ has a logarithmic singularity at the point a and it is bounded at the points b and d. At infinity, the function $\omega_1(\zeta)$ is bounded and it vanishes at the point $\zeta=e_1$.

Apart from the conditions at $\zeta=\infty$ and $\zeta=e_1$, these conditions are the same as those for the function $\omega_1(\zeta)$ in the double-spiral-vortex model for a wedge beneath a free surface (Antipov & Zemlyanova 2009). Therefore, the function $\omega_1(\zeta)$ can be determined in a similar manner through the solution to a Riemann–Hilbert problem on a two-sheeted genus-1 Riemann surface, $\mathcal{R}$, of the algebraic function $u=p^{1/2}(\zeta)$, $\zeta\in\mathcal{C}_1$, and $u=-p^{1/2}(\zeta)$, $\zeta\in\mathcal{C}_2$. Here $\mathcal{C}_1$ and $\mathcal{C}_2$ are two replicas of the extended ζ-plane with the cuts l_0 and l_1. We write down only the final formulas for the solution. Let $\Phi(\zeta,u)=-i\omega_1(\zeta)$ on the upper sheet $\mathcal{C}_1$ and $\Phi(\zeta,u)=i\overline{\omega_1(\bar\zeta)}$ on the lower sheet $\mathcal{C}_2$. Then,

$$\Phi(\zeta,u)=X(\zeta,u)[\Psi(\zeta,u)+\Omega(\zeta,u)],\quad (\zeta,u)\in\mathcal{R}, \tag{3.10}$$

where

$$\begin{aligned} \Psi(\zeta,u)=&-\frac{\alpha}{2\pi i}\int_{ab}\frac{(1+u/v)\,\mathrm{d}\xi}{X^+(\xi,v)(\xi-\zeta)}+\frac{\pi-\beta}{2\pi i}\int_{da}\frac{(1+u/v)\,\mathrm{d}\xi}{X^+(\xi,v)(\xi-\zeta)}\\ &-\frac{\ln(\sigma+1)}{4\pi}\int_{bcd}\frac{(1+u/v)\,\mathrm{d}\xi}{X(\xi,v)(\xi-\zeta)},\quad v=u(\xi). \end{aligned} \tag{3.11}$$

The function $\Omega(\zeta,u)$ is a rational function on the surface $\mathcal{R}$ given by

$$\begin{aligned} \Omega(\zeta,u)=&iM_0\frac{u(\zeta)+u(c)}{\zeta-c}+(M_1+iM_2)\frac{u(\zeta)+u(\eta_0)}{\zeta-\eta_0}\\ &-(M_1-iM_2)\frac{u(\zeta)-\overline{u(\eta_0)}}{\zeta-\bar\eta_0}+M_3, \end{aligned} \tag{3.12}$$

where M_j $(j=0,1,2,3)$ are real constants to be fixed.

As for the function $X(\zeta,u)$, it is a piece-wise meromorphic function, symmetric on the surface, $X(\zeta,u)=\overline{X(\bar\zeta,-u(\bar\zeta))}$, $(\zeta,u)\in\mathcal{R}\setminus\mathcal{L}$, $\mathcal{L}=l_0\cup l_1$, discontinuous through the contour $dab\in\mathcal{R}$ and whose one-sided limits satisfy the boundary condition $X^+(\xi,v)=-X^-(\xi,v)$, $(\xi,v)\in dab$. This function is defined by singular integrals

$$\begin{aligned} X(\zeta,u)=\exp\Bigg\{&\frac{1}{4}\int_{dab}\left(1+\frac{u(\zeta)}{u(\xi)}\right)\frac{\mathrm{d}\xi}{\xi-\zeta}-\frac{1}{2}\int_{\gamma}\left(1+\frac{u(\zeta)}{u(\xi)}\right)\frac{\mathrm{d}\xi}{\xi-\zeta}\\ &-\frac{1}{2}\int_{\gamma}\left(1-\frac{u(\zeta)}{\overline{u(\xi)}}\right)\frac{\mathrm{d}\bar\xi}{\bar\xi-\zeta}-2n_a\int_{l_0^+}\frac{u(\zeta)}{u(\xi)}\frac{\mathrm{d}\xi}{\xi-\zeta}\Bigg\}, \end{aligned} \tag{3.13}$$

where γ is a continuous curve whose starting and terminal points are $\boldsymbol{\eta}_0 = (\eta_0, u(\eta_0))$ and $\boldsymbol{\zeta}_0 = (\zeta_0, u(\zeta_0))$, respectively. The point $\boldsymbol{\eta}_0$ is an arbitrary fixed point lying on the upper sheet $\mathcal{C}_1$, while the point $\boldsymbol{\zeta}_0$ can lie on either sheet. The affix ζ_0 of the starting point is defined by

$$\zeta_0 = \sin^2 \frac{ig_0}{2k}, \tag{3.14}$$

where

$$k = m^{-1/2}, \quad g_0 = \frac{1}{4}\int_{dab} \frac{\mathrm{d}\xi}{p^{1/2}(\xi)} + \int_0^{\eta_0} \frac{\mathrm{d}\xi}{p^{1/2}(\xi)}. \tag{3.15}$$

Denote

$$I_{\pm} = \frac{1}{4}\int_{dab} \frac{\mathrm{d}\xi}{p^{1/2}(\xi)} + \int_0^{\eta_0} \frac{\mathrm{d}\xi}{p^{1/2}(\xi)} \pm \int_0^{\zeta_0} \frac{\mathrm{d}\xi}{p^{1/2}(\xi)}. \tag{3.16}$$

If it turns out that both the numbers

$$-\frac{\operatorname{Im} I_-}{4k\mathbf{K}} \quad \text{and} \quad \frac{\operatorname{Re} I_-}{4k\mathbf{K}'} \tag{3.17}$$

are integers, then the point $\boldsymbol{\zeta}_0 \in \mathcal{C}_1$ and $n_a = -\operatorname{Im} I_-(4k\mathbf{K})^{-1}$. Otherwise, the point $\boldsymbol{\zeta}_0$ falls on the lower sheet $\mathcal{C}_2$ and $n_a = -\operatorname{Im} I_+(4k\mathbf{K})^{-1}$. Here, $\mathbf{K} = \mathbf{K}(k)$ is the complete elliptic integral of the first kind, and $\mathbf{K}' = \mathbf{K}(\sqrt{1-k^2})$.

The curve γ does not cross the contour l_0. In the case $\boldsymbol{\zeta}_0 \in \mathcal{C}_2$, it passes through the point $\zeta = 0$ and consists of two parts, $\boldsymbol{\eta}_0\,\mathbf{0} \subset \mathcal{C}_1$ and $\mathbf{0}\,\boldsymbol{\zeta}_0 \subset \mathcal{C}_2$. If the point $\boldsymbol{\zeta}_0$ lies on the upper sheet, then the contour γ can be chosen as the straight line joining the points $\boldsymbol{\eta}_0$ and $\boldsymbol{\zeta}_0$ provided it does not cross the contour l_0. We notice that in all the numerical tests implemented, the point $\boldsymbol{\zeta}_0 \in \mathcal{C}_1$.

The solution (3.10) possesses 10 unknown real constants. They are M_0, M_1, M_2 and M_3 (the coefficients in the representation of the rational function $\Omega(\zeta, u)$), the angle of yaw δ and the points a, b, d, e_0 and m. To fix these unknowns, we have the same number of equations, linear and nonlinear. The first equation (3.8) links the three parameters a, e_0 and m. Write down the other equations. Owing to the simple pole of the function $X(\zeta, u)$ at the point $\boldsymbol{\zeta}_0$, the function $\omega_1(\zeta)$ has an inadmissible pole at this point. It becomes a removable singularity if the following complex condition holds:

$$\Psi(\zeta_0, u(\zeta_0)) + \Omega(\zeta_0, u(\zeta_0)) = 0. \tag{3.18}$$

To guarantee a smooth detachment of the jet breaking away from the wedge at the point $z = D$, we require

$$\Psi(d, u(d)) + \Omega(d, u(d)) = 0. \tag{3.19}$$

Notice that at the point $\zeta = b$, the solution is automatically bounded.

Since the function $\omega_1(\zeta)$ vanishes at the point $\zeta = e_1$, we impose the following condition:

$$\Psi(e_1, u(e_1)) + \Omega(e_1, u(e_1)) = 0. \tag{3.20}$$

Next, we wish the function $\omega_1(\zeta)$ being bounded at the infinite point. By analysing the principal term in equation (3.10) at infinity, we have

$$M_0 = \Psi_0 - 2M_2, \tag{3.21}$$

where Ψ_0 is a real constant given by

$$\Psi_0 = \frac{\alpha}{2\pi}\int_{ab}\frac{\mathrm{d}\xi}{vX^+(\xi,v)} - \frac{\pi-\beta}{2\pi}\int_{da}\frac{\mathrm{d}\xi}{vX^+(\xi,v)} + \frac{i\ln(\sigma+1)}{4\pi}\int_{bcd}\frac{\mathrm{d}\xi}{vX(\xi,v)}. \tag{3.22}$$

We also add the standard geometrical conditions

$$\lambda_1^\circ \sin\alpha - \Omega_1 = 0 \quad \text{and} \quad \lambda_2^\circ \sin\beta - \Omega_2 = 0, \tag{3.23}$$

where

$$\Omega_1 = \operatorname{Im}\int_{ab}\omega_0^*(\zeta)e^{-\omega_1(\zeta)}\,\mathrm{d}\zeta \quad \text{and} \quad \Omega_2 = \operatorname{Im}\int_{da}\omega_0^*(\zeta)e^{-\omega_1(\zeta)}\,\mathrm{d}\zeta. \tag{3.24}$$

The final two real equations come from the requirement for the mapping $z = f(\zeta)$ to satisfy the single-valuedness condition (3.4) or, equivalently, the following condition:

$$\int_{l_1^*}\omega_0^*(\zeta)e^{-\omega_1(\zeta)}\,\mathrm{d}\zeta = 0, \tag{3.25}$$

where l_1^* is a closed contour around the cut l_1 which does not cross the cut l_0.

Our next step is to determine the real constants $M_0,\dots,M_3$ and the angle of yaw $\delta = \alpha - \alpha_0$ explicitly from the linear equations (3.18)–(3.21). This can most conveniently be done by splitting the unknowns M_j as follows:

$$M_j = M_j^0 + \delta M_j^1, \quad j = 0,\dots,3. \tag{3.26}$$

We shall use, for brevity, the notations

$$\left.\begin{gathered}\rho_0(\zeta) = \frac{u(\zeta)+u(\eta_0)}{\zeta-\eta_0}, \quad \rho_1(\zeta) = \frac{u(\zeta)-\overline{u(\eta_0)}}{\zeta-\bar\eta_0}, \quad \rho_2(\zeta) = \frac{u(\zeta)+u(c)}{\zeta-c},\\ \Psi_1 = \Psi(\zeta_0,u(\zeta_0)), \quad \Psi_2 = \Psi(d,u(d)), \quad \Psi_3 = \Psi(e_1,u(e_1))\\ \text{and} \quad \Psi_j = \Psi_j^0 + \delta\Psi_j^1, \quad j = 0,\dots,3,\end{gathered}\right\} \tag{3.27}$$

where $\Psi_j^0 = \Psi_j|_{\alpha=\alpha_0,\beta=\beta_0}$, and the constants Ψ_j^1 coincide with Ψ_j if α and $\pi-\beta$ are replaced by 1 and -1, respectively. By applying the conditions (3.18)–(3.21), we express the angle of yaw through the constants M_j^ν as follows: $\delta = -\Delta_0/\Delta_1$, where

$$\Delta_\nu = \Psi_2^\nu + i\rho_2(d)M_0^\nu + [\rho_0(d)-\rho_1(d)]M_1^\nu + i[\rho_0(d)+\rho_1(d)]M_2^\nu + M_3^\nu, \quad \nu = 0,1. \tag{3.28}$$

The coefficients M_j^ν themselves are determined by

$$\left.\begin{aligned}&M_0^\nu = \Psi_0^\nu - 2M_2^\nu,\\ &M_3^\nu = -\Psi_3^\nu - iM_0^\nu\rho_2(e_1) - (M_1^\nu + iM_2^\nu)\rho_0(e_1) + (M_1^\nu - iM_2^\nu)\rho_1(e_1),\\ &M_1^\nu = \frac{1}{\Delta}(\Lambda_1^\nu \operatorname{Re}\mu_1 - \Lambda_2^\nu \operatorname{Im}\mu_1)\\ \text{and}\quad &M_2^\nu = -\frac{1}{\Delta}(\Lambda_2^\nu \operatorname{Re}\mu_2 + \Lambda_1^\nu \operatorname{Im}\mu_2),\end{aligned}\right\} \tag{3.29}$$

Table 1. The values of the parameters a, b, d, e_0, m and the yaw angle δ for the parameters (3.31) and some values of the cavitation number σ.

σ	a	b	d	e_0	$m-1$	δ
0.3	0.991565	0.996192	0.971464	1.0084579	1.395441×10^{-6}	0.129164
0.4	0.991764	0.996345	0.971563	1.008370	6.504862×10^{-6}	0.131272
0.6	0.960173	0.982899	0.862127	1.043103	1.561740×10^{-3}	0.134618
0.8	0.915786	0.965239	0.713255	1.100234	7.614774×10^{-3}	0.137920
1.0	0.870908	0.948976	0.570754	1.170520	1.958512×10^{-2}	0.141443

where

$$\left.\begin{aligned} \Delta &= \operatorname{Re}\mu_1 \operatorname{Re}\mu_2 + \operatorname{Im}\mu_1 \operatorname{Im}\mu_2, \\ \mu_1 &= \rho_0(\zeta_0) + \rho_1(\zeta_0) - 2\rho_2(\zeta_0) - \rho_0(e_1) - \rho_1(e_1) + 2\rho_2(e_1), \\ \mu_2 &= \rho_0(\zeta_0) - \rho_1(\zeta_0) - \rho_0(e_1) + \rho_1(e_1), \\ \Lambda_1^\nu &= \operatorname{Im}[\rho_2(\zeta_0) - \rho_2(e_1)]\Psi_0^\nu - \operatorname{Re}\Psi_1^\nu + \Psi_3^\nu \\ \text{and} \quad \Lambda_2^\nu &= \operatorname{Re}\rho_2(\zeta_0)\Psi_0^\nu + \operatorname{Im}\Psi_1^\nu, \quad \nu = 0, 1. \end{aligned}\right\} \tag{3.30}$$

The other unknown parameters of the conformal mapping, a, b, d, e_1 and m, can be found from a system of three real and one complex transcendental equations (3.8), (3.23) and (3.25).

(*d*) *Comparative analysis of the single- and double-spiral-vortex models*

The nonlinear system (3.8), (3.23) and (3.25) of five real equations is solved numerically by a technique based on the Newton method similarly to the system of four nonlinear equations associated with the problem for a wedge beneath a free surface (Antipov & Zemlyanova 2009). The main feature of the system (3.8), (3.23) and (3.25) is the presence of certain constraints for the unknown parameters. Indeed, we have chosen $a \in l_1^+$, have proved that $c = \bar{a} \in l_1^-$ and $1 < m < \infty$ by the definition. Therefore, $d \in l_1^\pm$, $b \in l_1^\pm$ and $0 < d < a$, $a < b < 1$. All numerical tests implemented show that, in fact, $d \in l_1^+$ and $b \in l_1^+$. It turns out that there are two sets of parameters of the conformal mapping, $\{a, b, d, e_1, m\}$ and $\{a, b, d, \bar{e}_1, m\}$, which satisfy the system of nonlinear equations. However, the set of parameters with $e_1 = e_0 - i0$ produces a non-physical solution: the two branches of the free streamline that define the cavity intersect each other, and the Brillouin condition is therefore violated.

For all the problem parameters tested, the physical solution corresponds to the case when $e_1 = e_0 + i0 \in l_0^+$ and therefore $e_2 = \bar{e}_1 \in l_0^-$. The values of the parameters of the conformal mapping and the angle of yaw for some values of the cavitation number σ when

$$\alpha_0 = \frac{\pi}{3}, \quad \beta_0 = \frac{2\pi}{3}, \quad \lambda_1 = 1, \quad \lambda_2 = 2, \quad h = 20 \quad \text{and} \quad h_1 = 10 \tag{3.31}$$

are given in table 1. It is seen that the angle of yaw increases when the cavitation number increases.

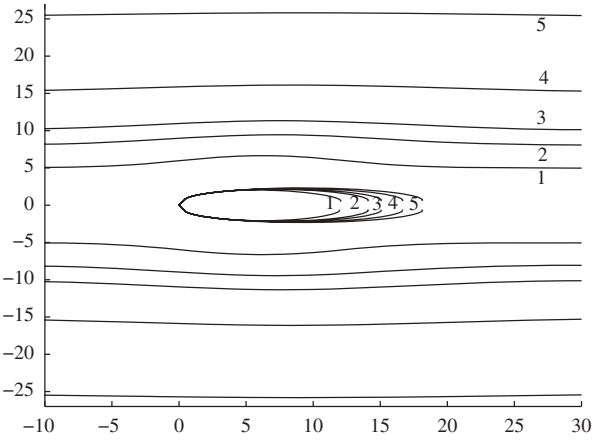

Figure 7. The cavity shape and the jet surface in the symmetric case when $\alpha_0 = \pi - \beta_0 = \pi/3$, $\lambda_1 = \lambda_2 = 1$ and $\sigma = 0.5$ for some values of h: $h = 10$ (1), $h = 16$ (2), $h = 20$ (3), $h = 30$ (4) and $h = 50$ (5).

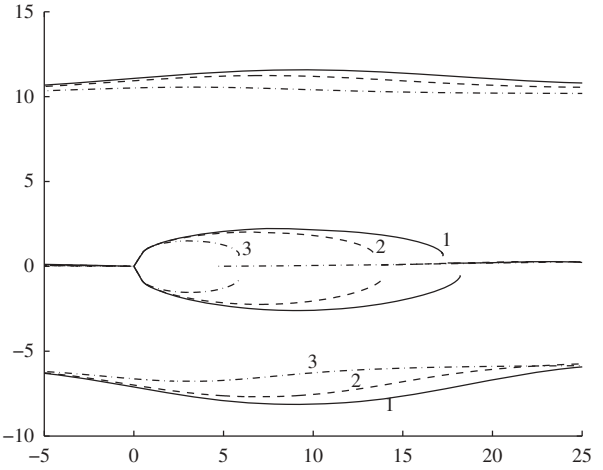

Figure 8. The cavity shape and the jet surface for $\alpha_0 = \pi - \beta_0 = \pi/3$, $\lambda_1 = \lambda_2 = 1$, $h = 16$ and $h_1 = 10$ when $\sigma = 0.4$ (1), $\sigma = 0.5$ (2) and $\sigma = 1$ (3).

To restore the shape of the cavity, we integrate the function $\mathrm{d}f/\mathrm{d}\zeta$ over the contours $b\tau$ ($\tau \in bc$) and $d\tau$ ($\tau \in dc$) as was described in the case of the double-spiral-vortex model in §2*c*. We have reconstructed the shape of the cavity behind the wedge and the jet for a symmetric wedge for different widths h of the jet or equivalently for different values of the parameter $\lambda_1^\circ = \lambda_2^\circ$ (figure 7). The numerical results show that when h grows and the cavitation number is fixed, the length of the cavity grows as well.

The jet boundary, the cavity shape and the streamline that splits at the vertex of the wedge and then emerges at the rear part of the cavity are shown in figure 8 for some cavitation numbers in the non-symmetric case. The amplitude of the wave on the surface of the jet and the cavity length increase when the cavitation number decreases.

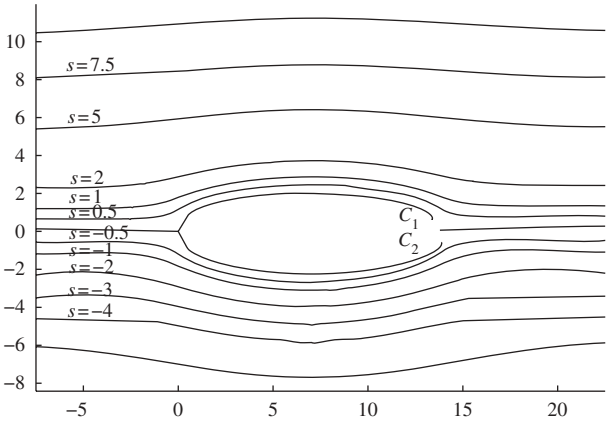

Figure 9. The streamlines $\psi(x, y) = s$ for some values of the constant s when $\alpha_0 = \pi/3$, $\beta_0 = 2\pi/3$, $\sigma = 0.5$, $h = 16$, $h_1 = 10$ and $\lambda_1 = \lambda_2 = 1$.

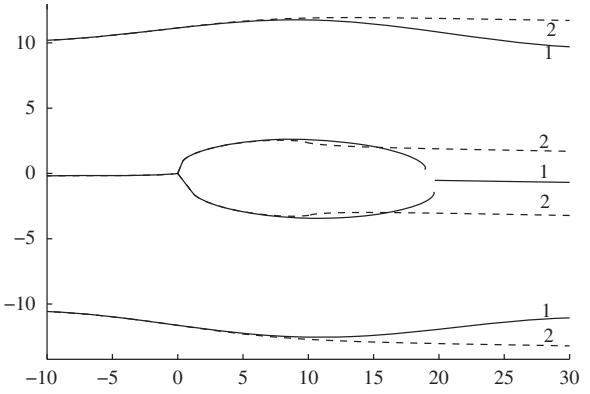

Figure 10. The cavity shape and the free surface when $\alpha_0 = \pi/3$, $\beta_0 = 2\pi/3$, $\sigma = 0.5$, $h = 20$, $h_1 = 10$, $\lambda_1 = 1$ and $\lambda_2 = 2$: the single-spiral-vortex model (solid line) and the double-spiral-vortex model (dashed line).

A flow map with several streamlines plotted is given in figure 9. As in the case of a wedge beneath a free surface (Antipov & Zemlyanova 2009), the streamline $\psi = 0$ and those that lie in close proximity to the cavity (they are not shown) spiral at the points C_1 and C_2. These streamlines are discontinuous in the physical plane in the neighbourhood of the point C (they are continuous in the Riemann surface of the flow). The other streamlines are continuous everywhere in the physical plane. The points C_1 and C_2 are determined as the images of the limit points c^+ and c^- (ζ approaches the point $c \in l_1^-$ from the right and the left, respectively). The position of the point C cannot be determined in a similar manner. We identify it as a point in the branch cut C_1C_2, say, as the midpoint of the segment C_1C_2, at which the streamline $\psi(x, y) = 0$ emerges from the infinite sheet of the Riemann surface of the model.

In figure 10, we present the cavity and jet profiles predicted according to the single-spiral-vortex model (a solid line) and the double-spiral-vortex model (a broken line). The shapes of the cavity computed according to the two models

Table 2. The angle of deflection ϵ of the jet at infinity for $\alpha_0 = \pi - \beta_0 = \pi/3$, $\lambda_1 = 1$, $\lambda_2 = 2$, $h = 20$, $h_1 = 10$.

σ	single-spiral-vortex model	double-spiral-vortex model
0.3	−0.01524	−0.01661
0.5	−0.02294	−0.01811
0.7	−0.02745	−0.01954
1.0	−0.03392	−0.02160

Table 3. Circulation $(V_\infty)^{-1}\Gamma$ for the single-spiral-vortex model: $\alpha_0 = \pi/3$, $\beta_0 = 2\pi/3$, $\lambda_1 = 1$, $\lambda_2 = 2$, $h = 20$, $h_1 = 10$.

σ	0.3	0.4	0.6	0.8	1.0
$(V_\infty)^{-1}\Gamma$	−10.454608	−5.668399	−1.094609	−0.873162	−0.792022

are different only at the rear part of the cavity. The length of the cavity is smaller for the double model; however, the separation point between the cavity and the wake is hardly noticeable. Also, the jet is wider for the double model.

The solid lines in figure 4 correspond to the drag and lift coefficients C_X and C_Y computed in the framework of the single-spiral-vortex model. It is seen that the curves for the single- and the double-spiral-vortex model (the broken lines) are very close to each other. In the non-symmetric case, as $x_1 \to +\infty$, the speed $V \to V_\infty$. The velocity vector $\mathbf{v}$ however does not tend to $(V_\infty, 0)$. This is because of the jet deflexion. In table 2, we give some values of the angle of deflection ϵ at infinity for both the models. It is small and of the same order for both the models.

Finally, we determine the circulation of the velocity around the closed contour $L_1 = ABCDA$ for the single-spiral-vortex model

$$\Gamma = \int_{l_1^*} \frac{\mathrm{d}w}{\mathrm{d}\zeta}\mathrm{d}\zeta = hV_\infty \int_{l_1^*} \tilde{\omega}_0(\zeta)\,\mathrm{d}\zeta. \tag{3.32}$$

It is seen from table 3 that for a non-symmetric wedge, the absolute values of the circulation, $|\Gamma|$, decrease when the cavitation number σ increases. As h increases and h_1 is fixed, Γ/V_∞ decreases: for $h_1 = 10$, $\lambda_1 = \lambda_2 = 1$, $\sigma = 0.5$, $\alpha_0 = \pi - \beta_0 = \pi/3$ and for $h = 30$, 80 and 150, we have $\Gamma/V_\infty = -0.4845$, -0.3520 and -0.3288, respectively, which is consistent with the results of Antipov & Zemlyanova (2009) for a wedge beneath a free surface. Because of the condition (2.5), the corresponding integral around the contour C_1DABC_2 for the double-spiral-vortex model is zero.

4. Conclusions

The main contribution of this work is the comparative analysis of the two nonlinear models by Tulin, the single- and double-spiral-vortex models applied to the problem for a jet past a yawed non-symmetric wedge.

By solving certain Riemann–Hilbert problems, we have derived the conformal mapping from a parametric half-plane onto the flow domain for the double-spiral-vortex model and from a plane cut along two segments, $[0,1]$ and $[m,\infty)$, onto the physical domain for the single-spiral-vortex model. The former case is simpler since the Riemann–Hilbert problem is set on the complex plane while it is formulated on a genus-1 Riemann surface in the case of the single-spiral-vortex model. In both models, the final step of the method is the solution of an associated system of transcendental equations for the unknown parameters of the conformal mapping. We have solved these systems by the Newton-type method. It turns out that the nonlinear system in the double-spiral-vortex model has a unique solution. For the single-spiral-vortex model, we have found two sets of parameters. However, one of them violates the Brillouin condition, which requires the free streamlines do not intersect each other. The second solution obeys all the conditions of the model and is therefore physical.

The numerical results for the drag and lift coefficients computed according to the single- and double-spiral-vortex models are very close. What is different is the shape of the rear part of the cavity, its length and also the profile of the jet. In general, the amplitude of the waves on the jet are higher in the double-spiral-vortex model. One of the assumptions of the double-spiral-vortex model used for numerical computations is that the complex potential is the same at the centres of the upper and lower vortices. This condition leads to a non-zero thickness of the wake at infinity. We have not analysed the model when this condition is replaced by the one that closes the wake at infinity.

This work was funded by NSF through grant DMS0707724.

Appendix A. Evaluation of the integral (2.17)

To evaluate the integral in equation (2.17), represent the function $\Phi(\zeta)$ in the form

$$\Phi(\zeta)=\chi(\zeta)\left\{\frac{\ln(1+\sigma)}{2\pi}[I(c_1,-1;\zeta)-I(b,c_2;\zeta)]-\frac{\pi-\beta}{\pi}I(-1,0;\zeta)+\frac{\alpha}{\pi}I(0,b;\zeta)\right\}, \tag{A 1}$$

where

$$I(d_1,d_2;\zeta)=\int_{d_1}^{d_2}\frac{\mathrm{d}\xi}{\sqrt{|(\xi-b)(\xi+1)|}(\xi-\zeta)}. \tag{A 2}$$

Let first $[d_1,d_2]=[c_1,-1]$. We make the substitutions $\xi=-(b+1)\tau-1$, $\zeta=-(b+1)t-1$ and $r_1=(-c_1-1)/(b+1)$, and then

$$\tau_*=\sqrt{\frac{1+\tau}{\tau}},\quad t_*=\sqrt{\frac{1+t}{t}}\quad\text{and}\quad \rho_1=\sqrt{\frac{1+r_1}{r_1}}=\sqrt{\frac{b-c_1}{-c_1-1}}, \tag{A 3}$$

where $\sqrt{(t+1)/t}$ is a fixed branch to be defined. This reduces the integral $I(c_1,-1;\zeta)$ to the following one:

$$I(c_1,-1;\zeta)=-\frac{1}{b+1}\left(\hat{\zeta}-\frac{1}{\hat{\zeta}}\right)\ln\frac{\rho_1-\hat{\zeta}}{\rho_1+\hat{\zeta}}, \tag{A 4}$$

where $\hat{\zeta}=\sqrt{(1+t)/t}=\sqrt{(b-\zeta)/(-\zeta-1)}$ is the branch defined in the ζ-plane cut along the segment $[-1,b]$ fixed by the condition $\sqrt{(b-\xi)/(-\xi-1)}>0$, $\xi<-1$. The branch of the logarithmic function in equation (A 4) is defined by the conditions $\arg(\rho_1\pm\zeta_1)\in[-\pi,\pi]$ and $\arg(\rho_1-\hat{\zeta})=\mp\pi$ when $\zeta=\xi\pm i0$, $c_1<\xi<-1$. By establishing the connection between the two functions

$$\hat{\zeta}-\frac{1}{\hat{\zeta}}=-\frac{b+1}{\chi(\zeta)}, \tag{A 5}$$

we obtain

$$I(c_1,-1;\zeta)=\frac{1}{\chi(\zeta)}\ln\frac{\rho_1-\hat{\zeta}}{\rho_1+\hat{\zeta}}. \tag{A 6}$$

Similarly, for the integral $I(b,c_2)$, we have

$$I(b,c_2;\zeta)=\frac{1}{\chi(\zeta)}\ln\frac{\rho_2-\tilde{\zeta}}{\rho_2+\tilde{\zeta}}, \tag{A 7}$$

where

$$\rho_2=\sqrt{\frac{c_2+1}{c_2-b}}\quad\text{and}\quad\tilde{\zeta}=\sqrt{\frac{\zeta+1}{\zeta-b}}=\frac{1}{\hat{\zeta}}. \tag{A 8}$$

To evaluate the integral $I(-1,0;\zeta)$, we make the substitutions $\tau=(\xi+1)/(b+1)$, $t=(\zeta+1)/(b+1)$, and then $\tau_*=\sqrt{(1-\tau)/\tau}$, $t_*=\sqrt{(1-t)/t}$. Ultimately, we find

$$I(-1,0;\zeta)=\frac{i}{\chi(\zeta)}\ln\frac{\sqrt{b}-\zeta^\circ}{\sqrt{b}+\zeta^\circ}. \tag{A 9}$$

Here

$$\zeta^\circ=\pm\sqrt{\left|\frac{b-\xi}{1+\xi}\right|}\quad\text{and}\quad\zeta=\xi\pm i0,\ -1<\xi<0. \tag{A 10}$$

Similarly,

$$I(0,b;\zeta)=-\frac{\pi}{\chi(\zeta)}-\frac{i}{\chi(\zeta)}\ln\frac{\sqrt{b}-\zeta^\circ}{\sqrt{b}+\zeta^\circ}. \tag{A 11}$$

Consequently, the function $\Phi(\zeta)$ has the form

$$\Phi(\zeta)=\frac{\ln(1+\sigma)}{2\pi}\left(\ln\frac{\rho_1-\hat{\zeta}}{\rho_1+\hat{\zeta}}-\ln\frac{\rho_2-1/\hat{\zeta}}{\rho_2+1/\hat{\zeta}}\right)-\alpha-\frac{i(\pi+\alpha-\beta)}{\pi}\ln\frac{\sqrt{b}-\zeta^\circ}{\sqrt{b}+\zeta^\circ}. \tag{A 12}$$

By using the relations

$$\left.\begin{aligned}
\ln\frac{b_1-\hat{\zeta}}{b_1+\hat{\zeta}} &= \mp\pi i+\ln\left|\frac{b_1-\hat{\zeta}}{b_1+\hat{\zeta}}\right|, \quad \zeta=\xi+\pm i0, \quad c_1<\xi<-1,\\
\ln\frac{b_2-1/\hat{\zeta}}{b_2+1/\hat{\zeta}} &= \pm\pi i+\ln\left|\frac{b_2-1/\hat{\zeta}}{b_2+1/\hat{\zeta}}\right|, \quad \zeta=\xi+\pm i0, \quad b<\xi<c_2,\\
\text{and}\qquad \ln\frac{\sqrt{b}-\zeta^\circ}{\sqrt{b}+\zeta^\circ} &= \begin{pmatrix}\pi i\\ 0\end{pmatrix}\pm\ln\left|\frac{\sqrt{b}-\zeta^\circ}{\sqrt{b}+\zeta^\circ}\right|, \quad \zeta=\xi+\pm i0, \quad \begin{pmatrix}-1<\xi<0\\ 0<\xi<b\end{pmatrix},
\end{aligned}\right\} \tag{A 13}$$

we can verify that the function (A 12) satisfies the boundary condition of the Riemann–Hilbert problem (2.15).

References

Antipov, Y. A. & Silvestrov, V. V. 2007 Method of Riemann surfaces in the study of supercavitating flow around two hydrofoils in a channel. *Physica D* **235**, 72–81. (doi:10.1016/j.physd.2007.04.013)

Antipov, Y. A. & Silvestrov, V. V. 2008 Double cavity flow past a wedge. *Proc. R. Soc. A* **464**, 3021–3038. (doi:10.1098/rspa.2008.0136)

Antipov, Y. A. & Silvestrov, V. V. 2009 Circular map for supercavitating flow in a multiply connected domain. *Quart. J. Mech. Appl. Math.* **62**, 167–200. (doi:10.1093/qjmam/hbp003)

Antipov, Y. A. & Zemlyanova, A. Y. 2009 Motion of a yawed supercavitating wedge beneath a free surface. *SIAM J. Appl. Math.* **70**, 923–948. (doi:10.1137/090747300)

Bassanini, P. & Elcrat, A. 1988 A univalent spiral-vortex model for separated flow past a polygonal obstacle. *ZAMP* **39**, 455–467. (doi:10.1007/BF00948957)

Brennen, C. E. 1985 *Cavitation and bubble dynamics*. Oxford, UK: Oxford University Press.

Furuya, O. 1975 Nonlinear calculation of arbitrary shaped supercavitating hydrofoils near a free surface. *J. Fluid Mech.* **68**, 21–40. (doi:10.1017/S0022112075000663)

Gilbarg, D. 1960 *Jets and cavities*. Handbuch der Physic, vol. 9, pp. 311–445. Berlin, Germany: Springer-Verlag.

Gurevich, M. I. 1979 *The theory of jets in an ideal fluid*. Moscow, Russia: Nauka.

Kawakami, E., Williams, M. & Arndt, R. E. A. 2009 Investigation of the behavior of ventilated supercavities. In *Proc. 7th Int. Symp. on Cavitation*, CAV2009 – Paper 111, Ann Arbor, MI.

Larock, B. & Street, R. 1967 Nonlinear solution for a fully cavitating hydrofoil beneath a free surface. *J. Ship Res.* **11**, 131–140.

Larock, B. & Street, R. 1975 A Riemann–Hilbert problem for nonlinear, fully cavitating flow. *J. Ship Res.* **9**, 170–178.

Terent'ev, A. G. 1976 Non-linear theory of cavitational flow around obstacles. *Fluid Dyn.* **11**, 142–145. (doi:10.1007/BF01023411)

Terent'ev, A. G. 1981 *Mathematical problems of cavitation*. Cheboksary, Russia: Chuvash State University.

Tulin, M. P. 1964 Supercavitating flows—small perturbation theory. *J. Ship Res.* **7**, 16–37.

Wu, T. Y. 1972 Cavity and wake flows. *Annu. Rev. Fluid Mech.* **4**, 243–284. (doi:10.1146/annurev.fl.04.010172.001331)